# Molecular Siegert states in an electric field. II. Transverse momentum distribution of the ionized electrons

Vinh N. T. Pham,[1] Oleg I. Tolstikhin,[2,3] and Toru Morishita[1]

[1]*Department of Engineering Science, The University of Electro-Communications, 1-5-1 Chofu-ga-oka, Chofu-shi, Tokyo 182-8585, Japan*
[2]*National Research Center "Kurchatov Institute", Kurchatov Square 1, Moscow 123182, Russia*
[3]*Moscow Institute of Physics and Technology, Dolgoprudny 141700, Russia*

This paper completes our previous studies of atomic [P. A. Batishchev, O. I. Tolstikhin, and T. Morishita, Phys. Rev. A **82**, 023416 (2010)] and molecular [L. Hamonou, T. Morishita, and O. I. Tolstikhin, Phys. Rev. A **86**, 013412 (2012)] Siegert states (SSs) in an electric field by presenting illustrative calculations of the transverse momentum distribution (TMD) for a molecular potential. The method of adiabatic expansion in parabolic coordinates developed in this series for calculating the SSs is summarized. Its implementation is extended to the calculation of the normalized molecular SS eigenfunction, which is required for calculating the TMD. We consider a soft-core potential modeling the hydrogen molecular ion $H_2^+$. The behavior of the parabolic adiabatic potentials, channel functions and the total SS eigenfunction is illustrated, which was not included in the previous publications. The TMDs for the $1s\sigma$ and $2p\pi^\pm$ states are calculated. Their dependence on field and orientation of the molecule with respect to the field is compared with the predictions of the weak-field asymptotic theory. On the example of the even $2p\pi^+$ state, it is shown that TMD can rapidly change its shape in situations where there is no a single dominant ionization channel.

PACS number(s): 32.60.+i, 33.80.Rv, 42.50.Hz

## I. INTRODUCTION

In the general context of quantum mechanics, Siegert states (SSs) are regular eigensolutions of the stationary Schrödinger equation satisfying outgoing-wave boundary conditions in the asymptotic region [1]. The bound states of atoms and molecules turn into SSs in the presence of an external static electric field. The complex SS eigenvalue defines the Stark-shifted energy and ionization rate of the system in the field. The SS eigenfunction defines the transverse momentum distribution (TMD) of ionized electrons in the outgoing flux. The SS eigenvalue and TMD amplitude are two fundamental properties of atoms and molecules characterizing their interaction with a static electric field. The current interest in numerical [2,3] and analytical [4–6] methods to evaluate these properties is motivated by their applications in strong-field physics [7]. In particular, they are required for calculating photoelectron momentum distributions produced by intense low-frequency laser pulses within the adiabatic theory [8]. They are also needed for the analysis of experimental photoelectron and harmonic spectra [9–12].

Recently, we have developed a powerful method of adiabatic expansion in parabolic coordinates for calculating one-electron SSs in axially symmetric potentials [2] and general potentials without any symmetry [3]. Such potentials can be used to model atoms and molecules in the single-active-electron and frozen-nuclei approximations. Axially symmetric potentials correspond to atoms and linear molecules aligned along the field, and general potentials correspond to molecules arbitrarily oriented with respect to the field. The method reduces the three-dimensional stationary Schrödinger equation for the SSs to a multichannel eigenvalue problem in one variable, which can be efficiently solved by the slow variable discretization method [13] in combination with the $R$-matrix propagation technique [14]. This approach also enables one to construct the asymptotic solution of the SS eigenvalue problem in the weak-field limit. On this basis, the weak-field asymptotic theory (WFAT) of tunneling ionization of one-electron [4,5] and many-electron [6] systems was developed. In the atomic case [2], both the SS eigenvalue and TMD amplitude were treated in the formulation and illustrative calculations. The program developed in Ref. [2] was used in Ref. [8] for implementing the adiabatic theory. In the molecular case [3], the calculations become more laborious and so far were reported only for the SS eigenvalue. The formulation of the method for calculating the TMD amplitude in this case was given in Ref. [4]. The goal of this paper is to complete our previous studies of SSs [2,3] by presenting illustrative calculations of the TMD for a molecular potential.

The paper is organized as follows. In Sec. II we summarize basic equations of the theory of SSs in an electric field in the framework of the method of adiabatic expansion in parabolic coordinates [2–4]. In the present implementation of the method only one Coulomb singularity of the potential can be treated accurately. This is sufficient for considering realistic atomic potentials [2], but molecules should be described by soft-core potentials. We consider the same soft-core potential modeling the hydrogen molecular ion $H_2^+$ as in Ref. [3]. In Sec. III we present and discuss numerical results for the $1s\sigma$ and $2p\pi$ states in this potential. Since this is the concluding paper in the series [2,3] introducing the method, for completeness of the presentation and in order to illustrate the method we first discuss the behavior of the parabolic adiabatic potentials, channel functions, and the total SS eigenfunction, which was not included in the previous publications. Then we focus on the TMD and discuss its dependence on field and orientation of the molecule with respect to the field. The accurate numerical results are compared with the predictions of the WFAT [4]. Section IV concludes the paper.

## II. ADIABATIC EXPANSION
## IN PARABOLIC COORDINATES

We consider a molecule treated in the single-active-electron and frozen-nuclei approximations interacting with an external static uniform electric field $\mathbf{F} = F\mathbf{e}_z$, $F \geq 0$. The stationary Schrödinger equation for the active electron reads (atomic units are used throughout)

$$\left[ -\frac{1}{2} \Delta + V(\mathbf{r}) + Fz - E \right] \psi(\mathbf{r}) = 0. \quad (1)$$

The potential $V(\mathbf{r})$ describes the interaction with the parent molecular ion and implicitly depends on its shape determined by the internuclear configuration and orientation with respect to the field. The only assumption regarding $V(\mathbf{r})$ is

$$V(\mathbf{r})|_{r \to \infty} = -\frac{Z}{r}, \quad (2)$$

where $Z$ is the total charge of the parent ion. For $F = 0$, Eq. (1) has real-energy eigensolutions satisfying $\psi(\mathbf{r})|_{r \to \infty} = 0$, which represent bound states of the unperturbed molecule. For $F > 0$, these bound states turn into complex-energy SSs, which are the eigensolutions of Eq. (1) satisfying outgoing-wave boundary conditions in the asymptotic region. We solve Eq. (1) in parabolic coordinates defined by [15]

$$\xi = r + z, \quad 0 \leq \xi < \infty, \quad (3a)$$

$$\eta = r - z, \quad 0 \leq \eta < \infty, \quad (3b)$$

$$\varphi = \arctan \frac{y}{x}, \quad 0 \leq \varphi < 2\pi. \quad (3c)$$

To construct the SSs, we rewrite this equation in the form [2–4]

$$\left[ \frac{\partial}{\partial \eta} \eta \frac{\partial}{\partial \eta} + \mathcal{B}(\eta) + \frac{E\eta}{2} + \frac{F\eta^2}{4} \right] \psi(\mathbf{r}) = 0, \quad (4)$$

where the adiabatic Hamiltonian

$$\mathcal{B}(\eta) = \frac{\partial}{\partial \xi} \xi \frac{\partial}{\partial \xi} + \frac{\xi + \eta}{4\xi\eta} \frac{\partial^2}{\partial \varphi^2} - r V(\mathbf{r}) + \frac{E\xi}{2} - \frac{F\xi^2}{4} \quad (5)$$

is an operator acting on functions of $\xi$ and $\varphi$ and depending on $\eta$ as a parameter. This operator has a purely discrete spectrum. Its eigenvalues and eigenfunctions defined by

$$[\mathcal{B}(\eta) - \beta_\nu(\eta)]\Phi_\nu(\xi,\varphi;\eta) = 0, \quad (6a)$$

$$\Phi_\nu(\xi = 0,\varphi;\eta) < \infty, \quad \Phi_\nu(\xi \to \infty,\varphi;\eta) = 0, \quad (6b)$$

$$\Phi_\nu(\xi,\varphi + 2\pi;\eta) = \Phi_\nu(\xi,\varphi;\eta), \quad (6c)$$

also depend on $\eta$ as a parameter. For $F = 0$, the eigenvalues $\beta_\nu(\eta)$ are real and form a sequence unbounded from below

and the eigenfunctions $\Phi_\nu(\xi,\varphi;\eta)$ are chosen to be real. In this case, the solutions to Eqs. (6) can be enumerated by a single index $\nu = 1,2,\ldots$ in decreasing order of $\beta_\nu(\eta)$. By the analytic continuation in $F$, this enumeration can be applied for $F > 0$ when the eigenvalues $\beta_\nu(\eta)$ are complex, because the energy $E$ in Eq. (5) becomes complex. For any $\eta$, the different eigenfunctions are orthogonal and normalized by

$$\langle \Phi_\nu | \Phi_\mu \rangle \equiv \int_0^\infty \int_0^{2\pi} \Phi_\nu(\xi,\varphi;\eta)\Phi_\mu(\xi,\varphi;\eta) \, d\xi \, d\varphi = \delta_{\nu\mu}. \quad (7)$$

Note that there is no complex conjugation in this equation. The solutions to Eqs. (6) constitute the adiabatic basis. Taking into account Eq. (2), the adiabatic Hamiltonian ceases to depend on $\eta$ in the asymptotic region,

$$\mathcal{B} = \mathcal{B}(\eta)|_{\eta \to \infty} = \frac{\partial}{\partial \xi} \xi \frac{\partial}{\partial \xi} + \frac{1}{4\xi} \frac{\partial^2}{\partial \varphi^2} + Z + \frac{E\xi}{2} - \frac{F\xi^2}{4}. \quad (8)$$

The same holds for the solutions to Eqs. (6),

$$\beta_\nu = \beta_\nu(\eta)|_{\eta \to \infty}, \quad \Phi_\nu(\xi,\varphi) = \Phi_\nu(\xi,\varphi;\eta)|_{\eta \to \infty}. \quad (9)$$

The asymptotic channels are defined by

$$(\mathcal{B} - \beta_{n_\xi m})\Phi_{n_\xi m}(\xi,\varphi) = 0. \quad (10)$$

This equation allows separation of variables and has solutions of the form

$$\Phi_{n_\xi m}(\xi,\varphi) = \phi_{n_\xi m}(\xi) \frac{e^{im\varphi}}{\sqrt{2\pi}}, \quad (11)$$

where $\phi_{n_\xi m}(\xi)$ and the corresponding eigenvalues $\beta_{n_\xi m}$ are defined by

$$\left[ \frac{d}{d\xi} \xi \frac{d}{d\xi} - \frac{m^2}{4\xi} + Z + \frac{E\xi}{2} - \frac{F\xi^2}{4} - \beta_{n_\xi m} \right] \phi_{n_\xi m}(\xi) = 0, \quad (12a)$$

$$\phi_{n_\xi m}(\xi \to 0) \propto \xi^{|m|/2}, \quad \phi_{n_\xi m}(\xi \to \infty) = 0, \quad (12b)$$

$$\int_0^\infty \phi_{n_\xi m}(\xi)\phi_{n'_\xi m}(\xi) \, d\xi = \delta_{n_\xi n'_\xi}. \quad (12c)$$

Here $m = 0, \pm 1, \pm 2, \ldots$ is the azimuthal quantum number and $n_\xi = 0,1,2,\ldots$ enumerates the different solutions to Eqs. (12) for a given value of $m$. The functions (11) constitute the asymptotic basis. Note that the eigenvalues $\beta_{n_\xi m}$ do not depend on the sign of $m$, and hence the asymptotic states with $m \neq 0$ are doubly degenerate. The left-hand sides of Eqs. (9) are given by

$$\beta_\nu = \beta_{n_\xi |m|}, \quad (13a)$$

$$\Phi_\nu(\xi,\varphi) = \begin{cases} \Phi_{n_\xi 0}(\xi,\varphi), & m = 0, \\ \frac{e^{i(\lambda-1)\pi/4}}{\sqrt{2}}[c_{|m|}\Phi_{n_\xi,|m|}(\xi,\varphi) + \lambda c_{|m|}^*\Phi_{n_\xi,-|m|}(\xi,\varphi)], & m \neq 0, \end{cases} \quad (13b)$$

where $\lambda = \pm 1$ and the coefficients $c_{|m|}$ satisfy $|c_{|m|}|^2 = 1$. These coefficients are determined by the behavior of $V(\mathbf{r})$

at $\eta \to \infty$. Equations (13) show that in the asymptotic region the adiabatic channels can be enumerated by the

multi-index

$$\nu = (n_\xi, |m|, \lambda). \qquad (14)$$

By the analytic continuation in $\eta$, this classification by the asymptotic quantum numbers can be applied to all values of $\eta$. This provides an alternative way to label the solutions to Eqs. (6).

The solution to Eq. (4) is sought in the form of an expansion in the adiabatic basis,

$$\psi(\mathbf{r}) = \eta^{-1/2} \sum_\nu f_\nu(\eta) \Phi_\nu(\xi, \varphi; \eta). \qquad (15)$$

Substituting this into Eq. (4), one obtains a set of ordinary differential equations defining the unknown functions $f_\nu(\eta)$,

$$\left[ \frac{d^2}{d\eta^2} + \frac{1}{2} [E - U_\nu(\eta)] \right] f_\nu(\eta)$$
$$+ \sum_\mu \left[ 2P_{\nu\mu}(\eta) \frac{d}{d\eta} + Q_{\nu\mu}(\eta) \right] f_\mu(\eta) = 0, \quad (16)$$

where

$$U_\nu(\eta) = -\frac{1}{2\eta^2} - \frac{2\beta_\nu(\eta)}{\eta} - \frac{F\eta}{2} \qquad (17)$$

are the adiabatic potentials and the matrices

$$P_{\nu\mu}(\eta) = \left\langle \Phi_\nu \left| \frac{\partial \Phi_\mu}{\partial \eta} \right\rangle, \quad Q_{\nu\mu}(\eta) = \left\langle \Phi_\nu \left| \frac{\partial^2 \Phi_\mu}{\partial \eta^2} \right\rangle \qquad (18)$$

represent nonadiabatic couplings. Taking into account Eqs. (9), these matrices vanish in the asymptotic region. For $F > 0$ and $\arg F = 0$, the outgoing-wave solutions to the uncoupled equations satisfy [2–4]

$$f_\nu(\eta)|_{\eta \to \infty} = \frac{2^{1/2} f_\nu}{(F\eta)^{1/4}} \exp \left[ \frac{i F^{1/2} \eta^{3/2}}{3} + \frac{i E \eta^{1/2}}{F^{1/2}} \right]. \quad (19)$$

The SSs are represented by the solutions to Eqs. (16) satisfying regularity boundary conditions at $\eta \to 0$ and the outgoing-wave boundary conditions (19) at $\eta \to \infty$. Such solutions exist only for a discrete set of generally complex values of $E$—this is the SS eigenvalue problem. The real and imaginary parts of the SS eigenvalue $E$ define the energy $\mathcal{E}$ and ionization rate $\Gamma$ of the state,

$$E = \mathcal{E} - \frac{i}{2} \Gamma. \qquad (20)$$

The SS eigenfunction is normalized by

$$\int \psi^2(\mathbf{r}) \, d\mathbf{r} = \frac{1}{4} \int_0^\infty \int_0^\infty \int_0^{2\pi} \psi^2(\mathbf{r})(\xi + \eta) \, d\xi \, d\eta \, d\varphi = 1, \qquad (21)$$

where the integral should be regularized by deforming the integration path in $\eta$ from the real semiaxis into a contour in the complex $\eta$ plane [2]. We again note that there is no complex conjugation in Eq. (21), which is a general property of the theory of SSs. The unperturbed bound state, which coincides with the solution of the SS eigenvalue problem for $F = 0$, is denoted by $E_0$ and $\psi_0(\mathbf{r})$.

The outgoing-wave boundary condition for Eq. (1) can be written in the form [2,4]

$$\psi(\mathbf{r})|_{z \to -\infty} = \int A(\mathbf{k}_\perp) e^{i\mathbf{k}_\perp \mathbf{r}_\perp} g(z, k_\perp) \frac{d\mathbf{k}_\perp}{(2\pi)^2}, \qquad (22)$$

where $\mathbf{r}_\perp = (x, y) = (r_\perp \cos\varphi, r_\perp \sin\varphi)$, $\mathbf{k}_\perp = (k_x, k_y) = (k_\perp \cos\varphi_k, k_\perp \sin\varphi_k)$, and

$$g(z, k_\perp) = e^{-i\pi/12} 2\pi^{1/2} (2F)^{-1/6} \, \mathrm{Ai}(\zeta), \qquad (23a)$$

$$\zeta = \frac{2e^{-i\pi/3}}{(2F)^{2/3}} \left[ E - Fz - \frac{k_\perp^2}{2} \right]. \qquad (23b)$$

Here $\mathrm{Ai}(x)$ is the Airy function [16]. The function $g(z, k_\perp)$ contains only an outgoing wave as $z \to -\infty$, and $A(\mathbf{k}_\perp)$ is the amplitude of the TMD in the outgoing flux. This amplitude is given by [2,4]

$$A(\mathbf{k}_\perp) = \frac{2^{3/2} \pi i}{F^{1/2}} \sum_\nu f_\nu \Phi_\nu \left( \frac{k_\perp^2}{F}, \varphi_k \right). \qquad (24)$$

The TMD of the ionized electrons is

$$P(\mathbf{k}_\perp) \equiv |A(\mathbf{k}_\perp)|^2 = \frac{8\pi^2}{F} \left| \sum_\nu f_\nu \Phi_\nu \left( \frac{k_\perp^2}{F}, \varphi_k \right) \right|^2. \qquad (25)$$

The main objects of physical interest to be found in the calculations are the SS eigenvalue (20) and the TMD amplitude (24). Each step of the formulation must be implemented with high precision in order to obtain accurate results for these quantities.

## III. ILLUSTRATIVE RESULTS AND DISCUSSION

A numerical procedure implementing the method described above is documented in Refs. [2,3]. In Ref. [3] this procedure was used to calculate the SS eigenvalue for the hydrogen molecular ion $H_2^+$ modeled by the soft-core potential

$$V(\mathbf{r}) = -\frac{1}{\sqrt{|\mathbf{r} - \mathbf{R}/2|^2 + \epsilon}} - \frac{1}{\sqrt{|\mathbf{r} + \mathbf{R}/2|^2 + \epsilon}}. \qquad (26)$$

Here the nuclei are assumed to lie in the $xz$ plane, $\mathbf{R} = (R\sin\beta, 0, R\cos\beta)$, $R$ is the internuclear distance, $\beta$ is the angle between the internuclear axis and the electric field, and $\epsilon$ is the softening parameter. This potential satisfies Eq. (2) with $Z = 2$. In Ref. [3], the internuclear distance was set equal to its equilibrium value $R = 2$ and the softening parameter was chosen to be $\epsilon = 0.09$, which is small enough for the energies of the bound states be reasonably close to that in the pure Coulomb potential with $\epsilon = 0$. The potential (26) is symmetric with respect to the $xz$ plane, and the field does not break this symmetry. Therefore for the present model the solutions to Eq. (1) can be divided into even and odd with respect to the $xz$ plane. The even (odd) solutions are indicated by the superscript $+$ $(-)$. This superscript coincides with the value of $\lambda$ in Eq. (13b). All the coefficients $c_{|m|}$ in this case are equal to 1, so even and odd adiabatic channel functions $\Phi_\nu(\xi, \varphi; \eta)$ depend on $\varphi$ as $\cos(m\varphi)$ and $\sin(m\varphi)$, respectively. In the following, to avoid duplication in the notation, we omit $\lambda$ from the multi-index (14) and label the adiabatic channels by $\nu = (n_\xi, m)$, where $m \geq 0$. The unperturbed bound states in

the potential (26) are characterized by the projection $M$ of the electronic angular momentum on the internuclear axis. States with $M = 0$ ($\sigma$ states) are even; they are not degenerate, so the superscript $+$ in this case can be omitted. States with $M \neq 0$ are doubly degenerate, since their energy does not depend on the sign of $M$; the even and odd states discussed above are linear combinations of the degenerate states. In Ref. [3], to illustrate the different symmetry cases, the SSs originating from the unperturbed ground state $1s\sigma$ and two degenerate excited states $2p\pi^{\pm}$ were considered. The energies $\mathcal{E}$ and ionization rates $\Gamma$ of these states as functions of the field $F$ and orientation angle $\beta$ were calculated and compared with the predictions of perturbation theory [15] and the WFAT [4], respectively.

In the present work we extend the numerical procedure of Ref. [3] to the calculation of the normalized SS eigenfunction $\psi(\mathbf{r})$. This enables us to obtain the TMD amplitude (24). In the calculations reported below, we use the same potential (26) with the same values of $R$ and $\epsilon$ and consider the same states as in Ref. [3]. The goal of the calculations is to illustrate the field and orientation dependence of the TMD (25).

### A. Ground $1s\sigma$ state

We begin with the ground $1s\sigma$ state. The field-free energy of this state in the present soft-core model is $E_0 = -0.962\,366$, which is slightly higher than the corresponding energy $-1.102\,634$ for $\epsilon = 0$. The critical field $F_c$ giving a boundary between tunneling and over-the-barrier ionization regimes can be estimated as [3,4]

$$F_c = \frac{\varkappa^4}{8|2Z - \varkappa(m+1)|}, \qquad (27)$$

where $\varkappa = \sqrt{2|E_0|}$ and $m$ is the azimuthal quantum number of the dominant ionization channel. For the $1s\sigma$ state from Eq. (27) we obtain $F_c = 0.18$. In the calculations below we consider fields in the interval $0 \leq F \leq 0.3$, where the upper boundary is well above $F_c$.

#### 1. Adiabatic channels and the total SS eigenfunction

We use the $1s\sigma$ state as an example to illustrate the behavior of the different functions involved in the formulation of the present method. This information is helpful for understanding the method, but also provides a valuable insight into the underlying dynamics; for the sake of brevity, it was not included in our previous studies of SSs [2,3]. In this subsection we fix the orientation of the molecule at $\beta = 90°$. We discuss only the four lowest adiabatic channels with $\nu = (0,0)$, $(0,1)$, $(1,0)$, and $(0,2)$, but in the calculations, to achieve convergence of the results, 70 channels were coupled.

Figure 1 illustrates the behavior of the adiabatic potentials (17) as functions of $\eta$ for the four lowest adiabatic channels at two representative values of $F$. The potentials involve the eigenvalues $\beta_\nu(\eta)$ defined by Eqs. (6). The left panel shows the real part of the potentials. The horizontal lines indicate the energy $\mathcal{E}$ of the state. For the present state in the interval of $F$ considered and all orientation angles $\beta$, the lowest channel $(0,0)$ produces the dominant contribution to the expansion (15) for the SS eigenfunction (see Fig. 6 below). The evolution of the corresponding adiabatic potential with $F$ illustrates a
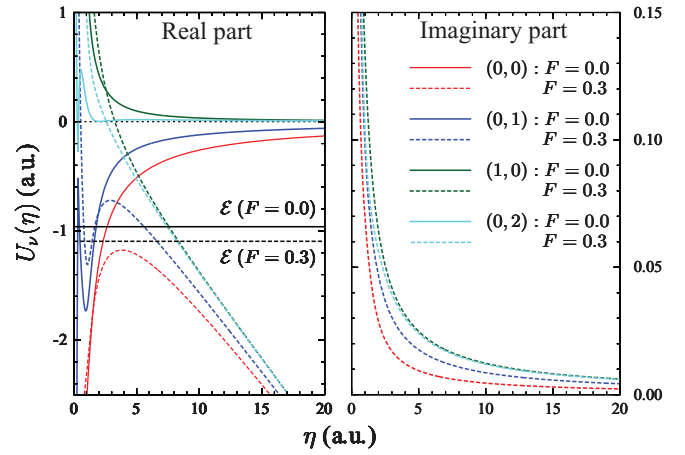


FIG. 1. (Color online) Adiabatic potentials (17) for the four lowest adiabatic channels $\nu = (n_\xi, m)$ in the $1s\sigma$ state at the orientation angle $\beta = 90°$. Solid (dashed) lines: results for $F = 0$ ($F = 0.3$). The horizontal (black) lines in the left panel show the real part $\mathcal{E}$ of the SS eigenvalue (20).

transition from the tunneling to the over-the-barrier ionization regime. For $F = 0$, the potential approaches 0 as $\eta \to \infty$, and the state is bound, since $\mathcal{E} < 0$. For $0 < F \ll F_c$, the behavior in the interval of $\eta$ shown in the figure remains similar to the case $F = 0$, but at larger $\eta$ the potential linearly goes down, because of the field term, and eventually becomes lower than $\mathcal{E}$. Now the electron can escape from the system by tunneling. This is the situation treated in the WFAT [4]. As $F$ grows further, the potential barrier becomes narrower and lower. For $F > F_c$ it becomes lower than $\mathcal{E}$, and then the electron can fly away through a classically accessible window over the barrier. This is the case for $F = 0.3$. We note that this simplified one-channel picture should not be taken too literally: one should remember that there exist non-negligible nonadiabatic couplings to other channels. The right panel of the figure presents the imaginary part of the potentials which originates from the imaginary part of the eigenvalues $\beta_\nu(\eta)$. The results are shown only for $F = 0.3$, since for $F = 0$ the eigenvalues are purely real. The curves monotonically approach 0 as $\eta$ grows and behave asymptotically as $1/\eta$.

Figure 2 illustrates the behavior of the adiabatic channel functions $\Phi_\nu(\xi, \varphi; \eta)$ for $F = 0$. In this case the functions are real. We consider the same four channels as in Fig. 1 at three representative values of $\eta$. The even solutions to Eqs. (6) as functions of the azimuthal angle $\varphi$ can be expanded in the basis of $\cos(m\varphi)$; this approach is indeed used in our numerical procedure [3]. The set $\eta = 0$ coincides with the positive half of the $z$ axis. Here only the $m = 0$ component exists in the expansion. Therefore the channel functions at $\eta = 0$ do not depend on $\varphi$. The set $\eta = 1$ is a paraboloid that passes through the inner regions of the potential well. Here the channel functions demonstrate strong dependence on $\varphi$, which corresponds to the presence of components with $m > 0$. For example, for channels $(0,0)$ and $(1,0)$ the component $m = 0$ still dominates, but the contribution from $m = 2$ becomes appreciable; the higher components remain small. The dominant components for channels $(0,1)$ and $(0,2)$ now are $m = 1$ and $m = 2$, respectively, instead of $m = 0$. The
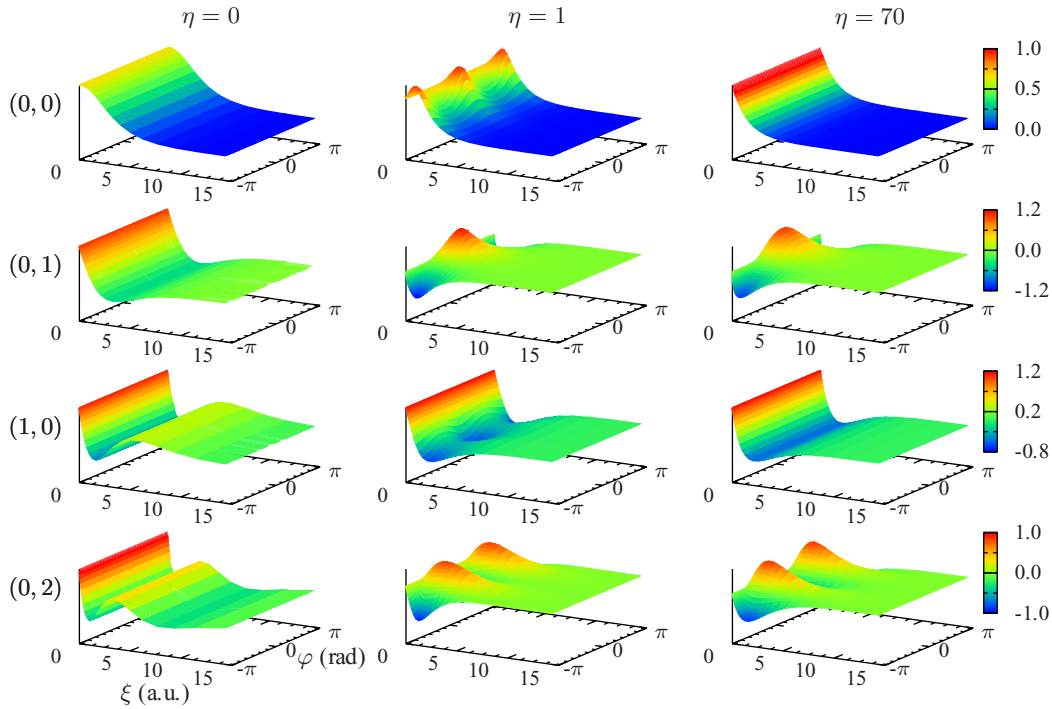
FIG. 2. (Color online) Channel functions $\Phi_\nu(\xi,\varphi;\eta)$ [see Eqs. (6)] for the same four adiabatic channels as in Fig. 1 at three representative values of $\eta$ in the field-free case, $F = 0$.

set $\eta = \text{const} \to \infty$ is a plane parallel to the $xy$ plane, which crosses the $z$ axis at $z = -\eta/2$. Here the channel functions acquire a separable form following from Eqs. (11) and (13b). Thus for channels (0,0) and (1,0) they become independent of $\varphi$, while for channels (0,1) and (0,2) they become proportional to $\cos\varphi$ and $\cos 2\varphi$, respectively. This asymptotic behavior of the channel functions is illustrated for $\eta = 70$. One can notice that the dependence of the channel functions on $\xi$ in the asymptotic region also agrees with their classification by parabolic quantum numbers $(n_\xi, m)$. The function (0,0) monotonically decays with $\xi$, the functions (0,1) and (0,2) have one zero at $\xi = 0$, and the function (1,0) turns zero at some intermediate value of $\xi$. For $F > 0$ the adiabatic channel functions become complex. Figure 3 illustrates the behavior of the real and imaginary parts of the lowest channel function for $F = 0.3$. This function and its evolution in $\eta$ look similar to the case $F = 0$ shown in the top row of Fig. 2. The same holds for the other channels, so we do not show them.

In the asymptotic region $\eta \to \infty$ the adiabatic channels are defined by the solutions to Eqs. (12). For $F = 0$, the solutions to this eigenvalue problem can be found analytically [4],

$$\beta_\nu^{(0)} = Z - \varkappa \left( n_\xi + \frac{|m| + 1}{2} \right), \tag{28a}$$

$$\phi_\nu^{(0)}(\xi) = \varkappa^{1/2} (\varkappa\xi)^{|m|/2} e^{-\varkappa\xi/2} \sqrt{\frac{n_\xi!}{(n_\xi + |m|)!}} L_{n_\xi}^{(|m|)}(\varkappa\xi), \tag{28b}$$

where $L_n^{(\alpha)}(x)$ are the generalized Laguerre polynomials [16]. For $F > 0$, the solutions become complex. Figure 4 illustrates the behavior of the asymptotic eigenvalues $\beta_\nu$ as functions of $F$ for the four channels discussed above. Figure 5 shows

the corresponding eigenfunctions $\phi_\nu(\xi)$ for two values of $F$. For sufficiently small $F$, the departure of the real parts of $\beta_\nu$ and $\phi_\nu(\xi)$ from their field-free values given by Eqs. (28) has power-series dependence on $F$ and can be described by perturbation theory [5]. Even for $F = 0.3$, which is in the over-the-barrier regime, this departure is rather small. The imaginary parts of $\beta_\nu$ and $\phi_\nu(\xi)$ originate from the imaginary part of the SS eigenvalue $E$ in Eq. (12a) which cannot be accounted for by perturbation theory. Their magnitudes grow exponentially with $F$ in the tunneling regime, and continue to grow, but less rapidly, in the over-the-barrier regime.

Having discussed the adiabatic channels, we now turn to the coefficient functions $f_\nu(\eta)$ in the expansion (15). These functions satisfy Eqs. (16) and the outgoing-wave boundary conditions (19). Figure 6 illustrates the behavior of $f_\nu(\eta)$ for two values of $F$. Note that for the $1s\sigma$ state at $\beta = 90°$ these functions for channels with odd $m$ identically vanish, because the SS eigenfunction in this case is even with respect to the $yz$ plane. This explains the absence of channel (0,1) in the figure. Also note that for both values of $F$ channel (0,0) dominates in the expansion (15). For $F = 0$, the functions $f_\nu(\eta)$ are localized in the potential well and rapidly decay beyond $\eta \approx 5$. For $F > 0$, they become delocalized. Their oscillatory behavior in the region $\eta \gtrsim 10$ represents the outgoing wave described by Eq. (19). The oscillations of the real and imaginary parts are shifted in phase by $\pi/2$, in accordance with Eq. (19). In the tunneling regime the amplitude of the outgoing wave is exponentially small in $F$ [4], but in the over-the-barrier regime shown in the figure it is similar to the values of $f_\nu(\eta)$ inside the potential well. By comparing $f_\nu(\eta)$ at large $\eta$ with Eq. (19) the asymptotic coefficients $f_\nu$ are obtained. Figure 7 illustrates the behavior of $f_\nu$ as functions of $F$. These coefficients are complex and their phase depends
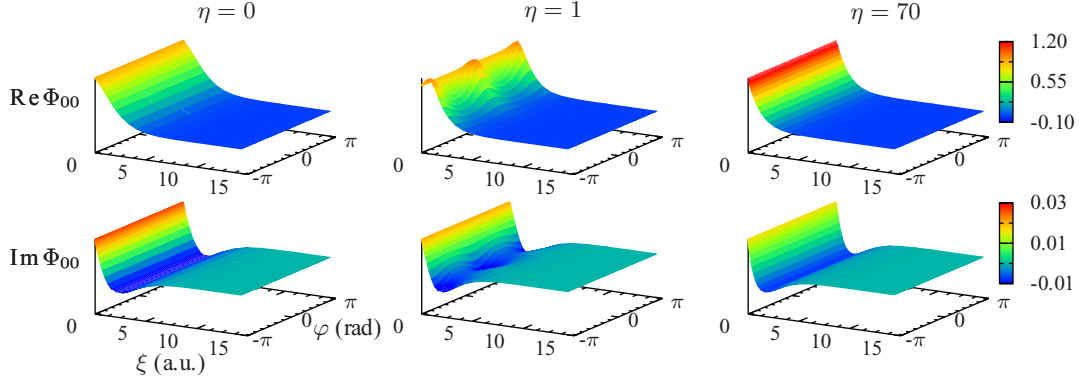
FIG. 3. (Color online) Channel function $\Phi_\nu(\xi,\varphi;\eta)$ for the lowest adiabatic channel $\nu = (0,0)$, as in the top row of Fig. 2, but for $F = 0.3$.

on $F$. Their absolute value squared gives the partial rate for ionization into the corresponding channel [4]. The ionization into channel (0,0) is seen to be dominant in the interval of $F$ considered.

We finally discuss the total SS eigenfunction $\psi(\mathbf{r})$. It is given by Eq. (15) as a function of parabolic coordinates $(\xi,\eta,\varphi)$. To illustrate its behavior in a two-dimensional figure, we average it over $\varphi$,

$$\bar{\psi}(\xi,\eta) = \frac{1}{2\pi} \int_0^{2\pi} \psi(\mathbf{r}) \, d\varphi. \tag{29}$$

Figure 8 shows this function for $F = 0$, when $\psi(\mathbf{r})$ coincides with the unperturbed bound state $\psi_0(\mathbf{r})$. In this case $\bar{\psi}(\xi,\eta)$ is real and rapidly decays as its arguments grow, as it should be for a bound state. The decay in $\xi$ and $\eta$ can be related to the corresponding behavior of the channel functions $\Phi_\nu(\xi,\varphi;\eta)$ and coefficient functions $f_\nu(\eta)$ shown in Figs. 2 and 6, respectively. Figure 9 shows $\bar{\psi}(\xi,\eta)$ for $F = 0.3$. Now the function is complex. It still decays in $\xi$, but has an outgoing wave as $\eta \to \infty$. Its oscillations approximately reproduce the behavior of $f_{00}(\eta)$ shown in Fig. 6, because channel (0,0) produces the dominant contribution to Eq. (15) in the present case.
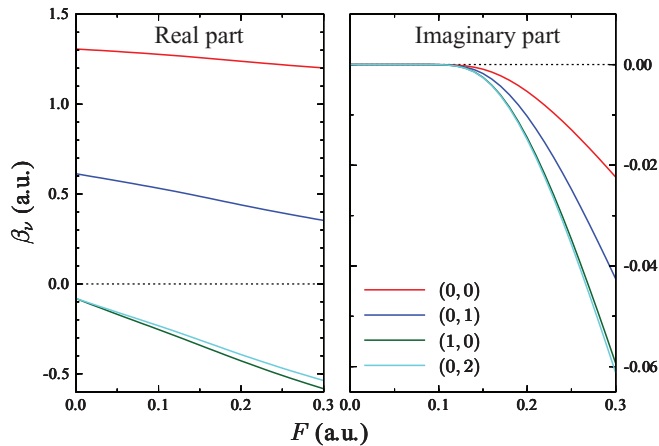
### 2. Transverse momentum distribution

We now turn to the discussion of the TMD for the $1s\sigma$ state. We consider $P(\mathbf{k}_\perp)$ defined by Eq. (25) as a function of either Cartesian $(k_x,k_y)$ or polar $(k_\perp,\varphi_k)$ coordinates in the plane of the transverse momentum $\mathbf{k}_\perp$ [the definitions are given below Eq. (22)]. The TMDs for atomic potentials in states with a certain value of the projection of the angular momentum on the field discussed in Ref. [2] are isotropic, i.e., do not depend on $\varphi_k$. Here we consider two-dimensional distributions in the plane $\mathbf{k}_\perp$. To understand the shape of the TMD, it is helpful to recall asymptotic results defining its behavior in the limit $F \to 0$. In the leading-order approximation of the WFAT the TMD is given by [4]

$$P_{as}(\mathbf{k}_\perp) = (2 - \delta_{m0})\Gamma_{as}\frac{4\pi}{F}\left[\phi_{0m}^{(0)}(k_\perp^2/F)\right]^2$$
$$\times \begin{cases} \cos^2(m\varphi_k), & \text{even states,} \\ \sin^2(m\varphi_k), & \text{odd states,} \end{cases} \tag{30}$$

where $\Gamma_{as}$ is the ionization rate,

$$\Gamma_{as} = (2 - \delta_{m0})|g_{0m}(\beta)|^2 W_{0m}(F). \tag{31}$$



FIG. 4. (Color online) Asymptotic eigenvalues $\beta_\nu$ [see Eqs. (12)] as functions of $F$ for the four lowest adiabatic channels $\nu = (n_\xi, m)$ in the $1s\sigma$ state at the orientation angle $\beta = 90°$.
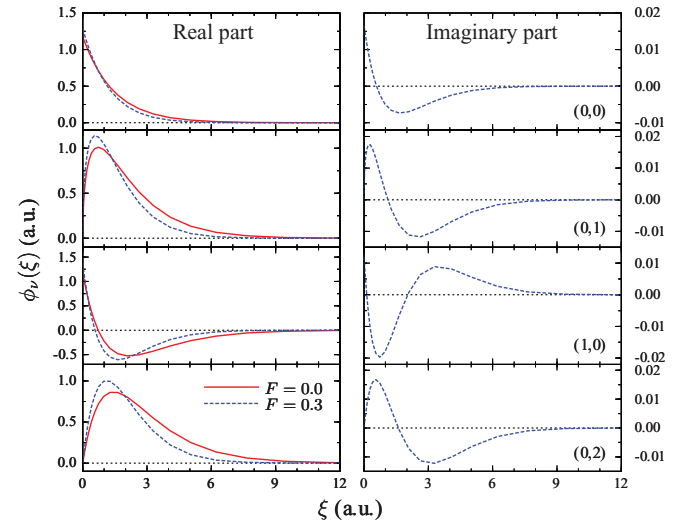


FIG. 5. (Color online) Asymptotic eigenfunctions $\phi_\nu(\xi)$ [see Eqs. (12)] for the same four adiabatic channels as in Fig. 4. Solid (dashed) lines: results for $F = 0$ ($F = 0.3$).
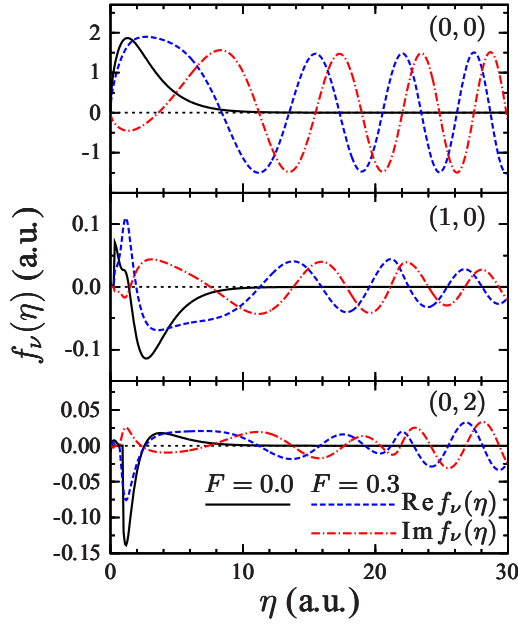
FIG. 6. (Color online) Coefficient functions $f_\nu(\eta)$ in Eq. (15) for the three lowest adiabatic channels $\nu = (n_\xi, m)$ contributing to the expansion [channel $(0,1)$ does not contribute] in the $1s\sigma$ state at the orientation angle $\beta = 90°$. Solid (dashed) lines: results for $F = 0$ ($F = 0.3$).

Here $g_{0m}$ is the asymptotic coefficient (which for the present nonpolar molecule coincides with the structure factor [17–19]),

$$g_{0m}(\beta) = \eta^{1+|m|/2-Z/\varkappa} e^{\varkappa\eta/2}$$
$$\times \int_0^\infty \int_0^{2\pi} \phi_{0m}^{(0)}(\xi) \frac{e^{-im\varphi}}{\sqrt{2\pi}} \psi_0(\mathbf{r}) d\xi d\varphi \bigg|_{\eta\to\infty}, \quad (32)$$
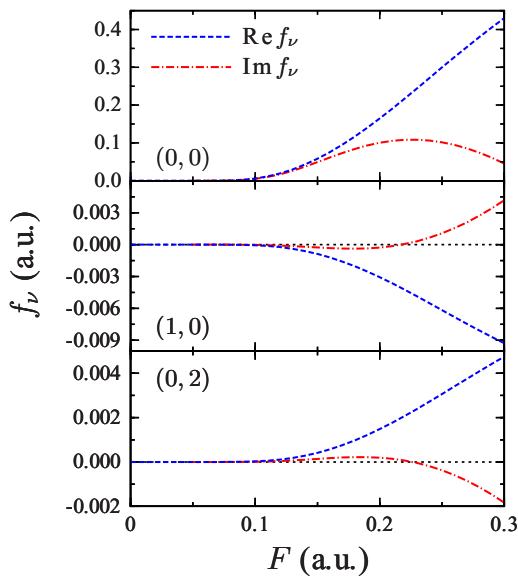


FIG. 7. (Color online) Asymptotic coefficients $f_\nu$ in Eq. (19) as functions of $F$ for the same channels as in Fig. 6.
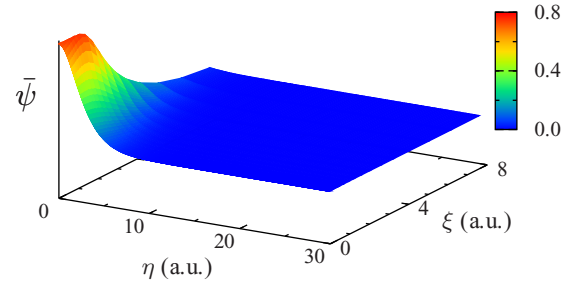


FIG. 8. (Color online) SS eigenfunction averaged over $\varphi$ [see Eq. (29)] in the $1s\sigma$ state at the orientation angle $\beta = 90°$ in the field-free case, $F = 0$.

$W_{0m}(F)$ is the field factor,

$$W_{0m}(F) = \frac{\varkappa}{2} \left(\frac{4\varkappa^2}{F}\right)^{2Z/\varkappa-|m|-1} \exp\left(-\frac{2\varkappa^3}{3F}\right), \quad (33)$$

and $m$ is the azimuthal quantum number for the dominant ionization channel. In this approximation the ionization rate is given in terms of the TMD by

$$\Gamma_{as} = \int P_{as}(\mathbf{k}_\perp) \frac{d\mathbf{k}_\perp}{(2\pi)^2}. \quad (34)$$

As a particular case of Eq. (30), one obtains the well-known isotropic Gaussian shape of the TMD for even states with $m = 0$ [20]

$$P_{as}(\mathbf{k}_\perp) = \Gamma_{as} \frac{4\pi\varkappa}{F} \exp\left(-\frac{\varkappa k_\perp^2}{F}\right). \quad (35)$$

For the present state the dominant ionization channel has $m = 0$, so Eq. (35) applies.

These equations show that the magnitude of the TMD is proportional to the ionization rate, and hence rapidly varies with $F$. To bring the vastly different results for the different values of $F$ to a common scale, we divide $P(\mathbf{k}_\perp)$ by

$$\mathcal{N} = F^{-1} \int P(\mathbf{k}_\perp) d\mathbf{k}_\perp, \quad (36)$$
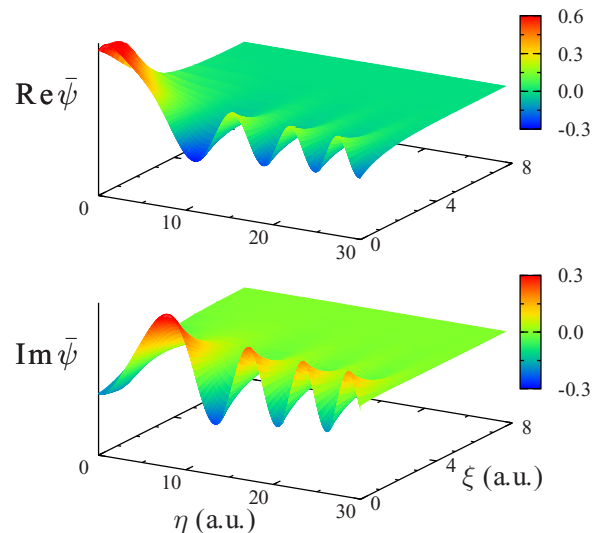


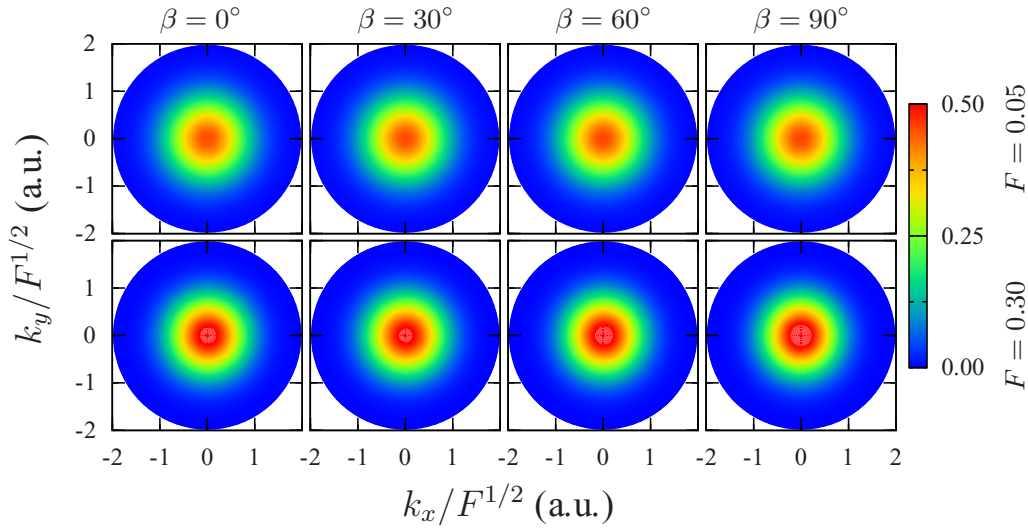FIG. 9. (Color online) Same as in Fig. 8, but for $F = 0.3$.

FIG. 10. (Color online) Normalized TMD $P(\mathbf{k}_\perp)/\mathcal{N}$ [see Eqs. (25) and (36)] as a function of the scaled transverse momentum $\mathbf{k}_\perp/F^{1/2}$ for the $1s\sigma$ state at several representative orientation angles $\beta$ and fields $F$.

and present thus defined *normalized* TMD as a function of the *scaled* transverse momentum $\mathbf{k}_\perp/F^{1/2}$. As follows from Eq. (34), within the WFAT the normalization factor (36) is given by $\mathcal{N}_{as} = (2\pi)^2 F^{-1}\Gamma_{as}$. Then from Eq. (30) one obtains that in the weak-field limit $P(\mathbf{k}_\perp)/\mathcal{N}$ as a function of $\mathbf{k}_\perp/F^{1/2}$ should not depend on $F$. Another goal of the normalization and scaling is to reveal a departure of the exact results from this prediction of the WFAT.

Figure 10 presents normalized TMDs at four orientation angles $\beta$ and two values of $F$. At all orientations, the TMDs look almost isotropic and have quite similar Gaussian-like shapes, in accordance with Eq. (35). However, a more careful inspection of the figure can detect some differences. To explore the differences, we show in Fig. 11 cuts of the TMDs as functions of $k_\perp/F^{1/2}$ along the ray $\varphi_k = 0$. For comparison, we also show the WFAT results obtained from Eq. (35) and divided by $\mathcal{N}_{as}$. For the weaker field $F = 0.05$, the exact results are in close agreement with Eq. (35), although there still is a small difference that depends on $\beta$. For the stronger field $F = 0.3$, the difference is more pronounced. One obvious strong-field effect is that the widths of the TMDs measured at half height become smaller. This is explained [2] by the role of the field term $F\xi^2/4$ in Eq. (12a). This term makes the functions $\phi_\nu(\xi)$ shrink towards $\xi = 0$ as $F$ grows (see the left column in Fig. 5). Therefore the asymptotic channel functions (13b) also shrink in $\xi$, which reduces the width of the TMD amplitude (24). We note that although the shapes of the normalized TMDs are in good agreement with the predictions of the WFAT, there is a big difference between the absolute magnitudes. For $F = 0.3$, for example, Eq. (35) overestimates the values of $P(\mathbf{k}_\perp)$ by about a factor of ten. This difference, however, originates from the difference between $\Gamma_{as}$ and the exact ionization rate $\Gamma$ (see Fig. 2 in Ref. [3]) and amounts to a common factor; it results in the different values of $\mathcal{N}_{as}$ and $\mathcal{N}$ and is canceled in the normalized representation.

There is also another strong-field effect, which manifests itself in the anisotropy of the TMDs at nonzero $\beta$ (for the present state at $\beta = 0°$, the TMD remains isotropic for all

fields). To make this anisotropy visible, we subtract from $P(\mathbf{k}_\perp)$ its average over $\varphi_k$,

$$\bar{P}(k_\perp) = \frac{1}{2\pi}\int_0^{2\pi} P(\mathbf{k}_\perp)\, d\varphi_k, \qquad (37)$$
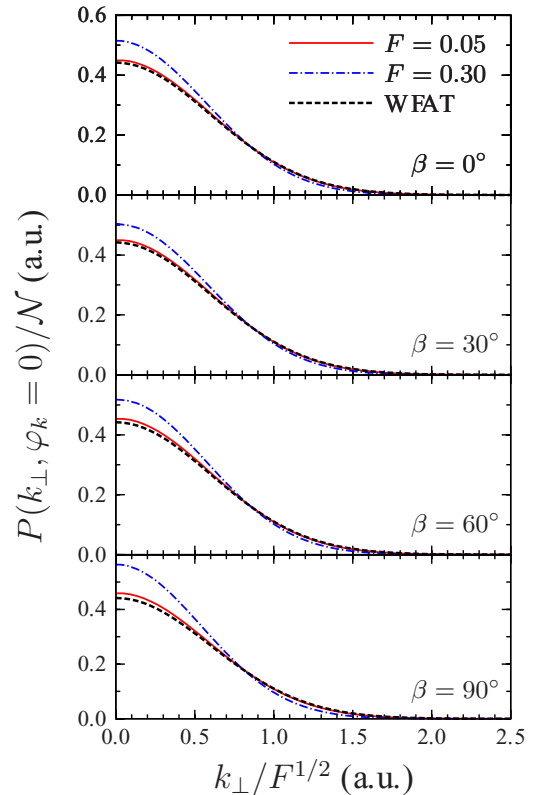


FIG. 11. (Color online) Cuts of the normalized TMDs shown in Fig. 10 along the ray $\varphi_k = 0$. Dashed (black) lines: the leading-order WFAT results obtained from Eq. (35) divided by $\mathcal{N}_{as}$.
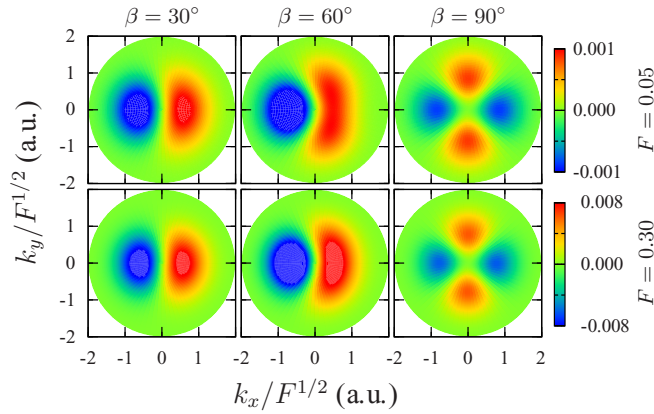
FIG. 12. (Color online) Normalized anisotropic part $[P(\mathbf{k}_\perp) - \bar{P}(k_\perp)]/\mathcal{N}$ [see Eq. (37)] of the TMDs shown in Fig. 10.

and again divide the difference by $\mathcal{N}$. The results are shown in Fig. 12. The subtraction eliminates the isotropic contribution from the dominant channel (0,0) and reveals small contributions from higher channels with nonzero $m$, which depend on $\varphi_k$. The anisotropy of the TMD reflects the symmetry of the SS eigenfunction. For all orientations, the SS is even with respect to the $xz$ plane, and so is the TMD. At small $\beta$, the main correction to the dominant isotropic term in Eq. (24) comes from channel (0,1), whose contribution is $\propto \cos \varphi_k$. But at $\beta = 90°$ the coefficient of this term vanishes, because at this orientation the SS acquires an additional symmetry—the SS eigenfunction is even with respect to the $yz$ plane. In this case the main correction comes from channel (0,2) and is $\propto \cos 2\varphi_k$. Figure 12 illustrates this evolution of the anisotropic part of the TMD with the variation of $\beta$. It also shows that the magnitude of the anisotropic part grows with $F$.

To summarize, although the TMDs shown in Fig. 10 look like what one would expect from Eq. (35), there exist

strong-field effects resulting in the deviation of their magnitudes and shapes from the predictions of the leading-order WFAT [4]. The difference in magnitudes is accounted for by the difference between the exact and WFAT ionization rates; it grows with $F$ and becomes large for $F \gtrsim F_c$. The difference in shapes is seen in a smaller width of the TMD and the appearance of anisotropy. For the $1s\sigma$ state, these deviations, however, remain rather small even for an over-the-barrier field $F = 0.3$.

### B. Excited $2p\pi^\pm$ states

We now consider the $2p\pi^\pm$ states. For $F = 0$ these states are degenerate. Their energy in the present soft-core model is $E_0 = -0.418\,947$ [21], which is again slightly higher than the corresponding energy $-0.428\,772$ for $\epsilon = 0$. For the $2p\pi^+$ state at $\beta \neq 0°$, the dominant channel is (0,0) and the critical field estimated using Eq. (27) is $F_c = 0.029$. For the $2p\pi^+$ state at $\beta = 0°$ and the $2p\pi^-$ state at any $\beta$, the dominant channel is (0,1) and the critical field is $F_c = 0.042$. We discuss the TMDs for these states in the interval of fields up to $F = 0.07$, which is well above the critical fields.

We first consider the even $2p\pi^+$ state. Figure 13 shows the normalized TMDs for this state at several representative values of the orientation angle $\beta$ and field $F$. The main difference from the results for the $1s\sigma$ state shown in Fig. 10 is that now the TMD changes its shape as $\beta$ and $F$ vary. For the parallel geometry, $\beta = 0°$, the dominant channel is (0,1). As follows from Eq. (30), the TMD in this case is $\propto \cos^2 \varphi_k$. Its nodal line at $\varphi_k = \pm\pi/2$ reflects the nodal plane $yz$ of the SS eigenfunction. At sufficiently large angles $\beta$ for a given field $F$, the dominant channel is (0,0). Then the TMD becomes almost isotropic and acquires a Gaussian-like shape, in accordance with Eq. (35). This is the case for $\beta = 60°$ and $90°$. The change of the dominant channel for a given $F$ occurs at a critical angle $\beta_c(F) \propto F^{1/2}$ [3,17]. At $\beta \approx \beta_c(F)$, the contributions from
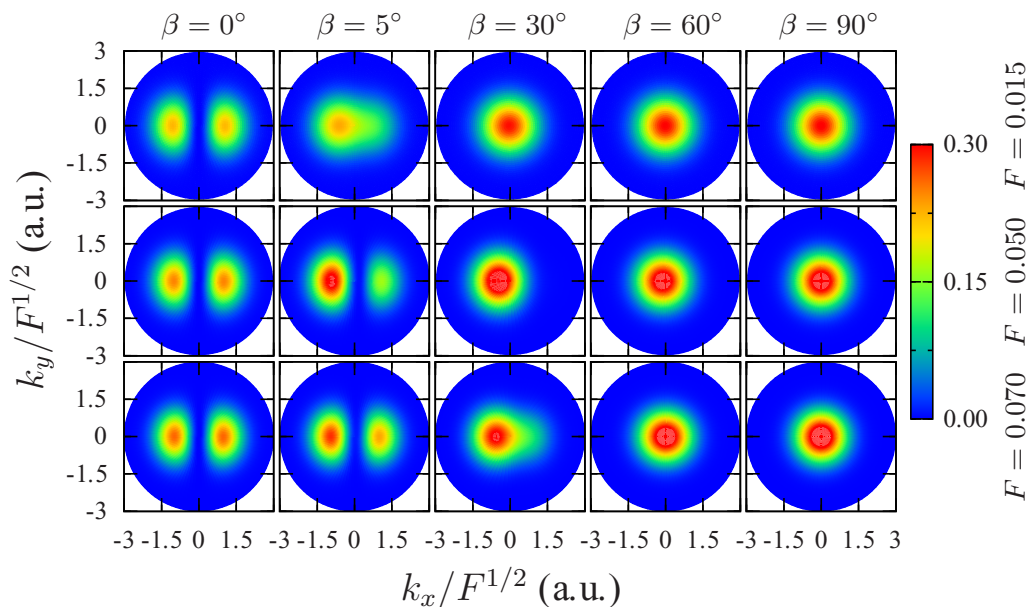


FIG. 13. (Color online) Normalized TMD $P(\mathbf{k}_\perp)/\mathcal{N}$ as a function of the scaled transverse momentum $\mathbf{k}_\perp/F^{1/2}$ for the $2p\pi^+$ state at several representative orientation angles $\beta$ and fields $F$.
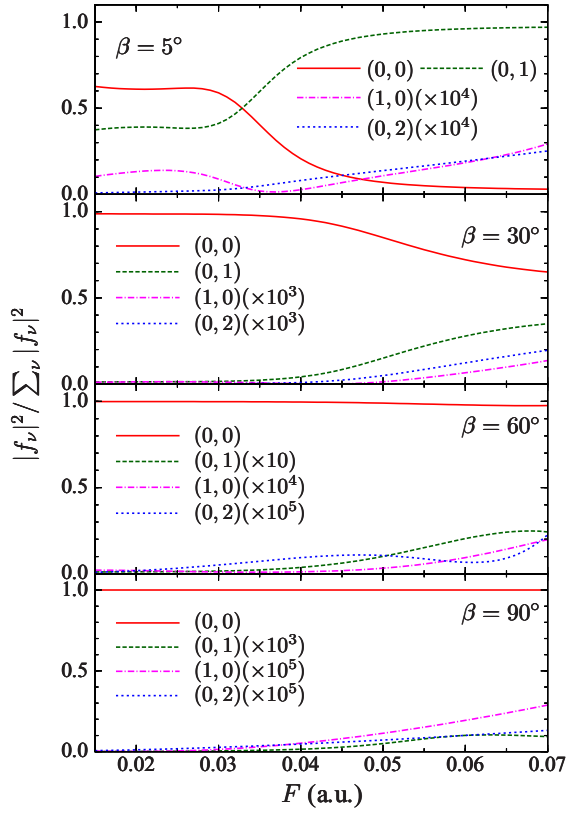
FIG. 14. (Color online) The asymptotic coefficients $f_\nu$ in Eq. (19), squared and normalized, as functions of $F$ for the $2p\pi^+$ state.
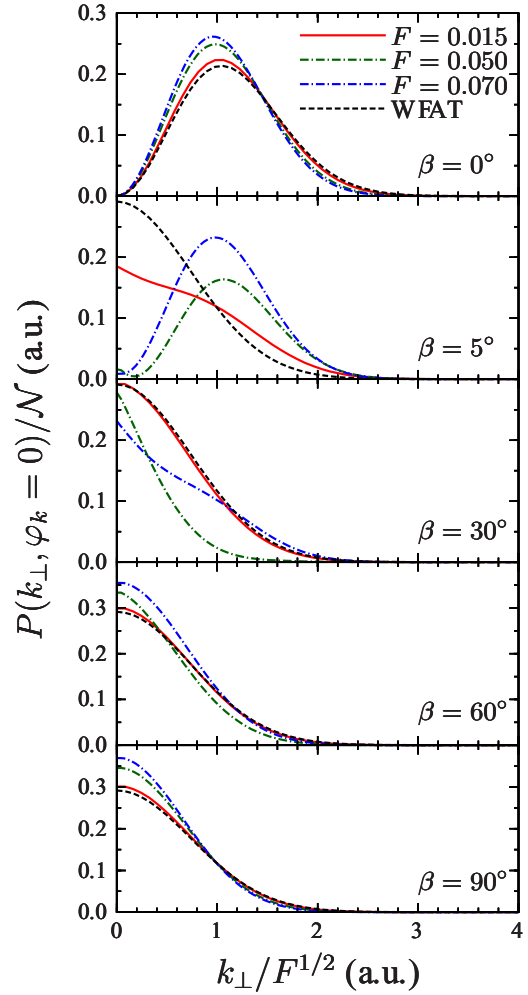


FIG. 15. (Color online) Cuts of the normalized TMDs shown in Fig. 13 along the ray $\varphi_k = 0$. Dashed (black) lines: the leading-order WFAT results obtained from Eq. (30) divided by $\mathcal{N}_{as}$.

channels $(0,0)$ and $(0,1)$ to the ionization flux are comparable. The interplay of these competing ionization channels causes the rapid variation of the shape of the TMD seen in the results for $\beta = 5°$ and $30°$.

Figure 14 illustrates the same interplay from a different side. The relative role of the different channels in Eq. (24) is determined by the coefficients $f_\nu$. The figure shows the behavior of these coefficients, squared and properly normalized, as functions of $F$. We consider the same values of $\beta$ as in Fig. 13 except for $\beta = 0°$, because in this case $f_{00} = 0$ for all values of $F$. At all $\beta$, only channels $(0,0)$ and $(0,1)$ produce non-negligible contributions to the TMD. At $\beta = 5°$, their contributions are comparable. Which of the channels dominates depends on $F$. The crossover occurs at $F \approx 0.033$; thus, for this field the critical angle is $\beta_c = 5°$. At $\beta = 30°$, channel $(0,0)$ is dominant in the interval of $F$ considered, but the contribution from channel $(0,1)$ is still appreciable. As $\beta$ grows, the relative role of channel $(0,1)$ decreases, and at $\beta = 90°$ channel $(0,0)$ remains the only dominant channel.

To compare the TMDs shown in Fig. 13 with the WFAT, we again consider their cuts along the ray $\varphi_k = 0$. The cuts are shown in Fig. 15. The WFAT results are obtained from Eq. (30) for even states with $m = 1$, for $\beta = 0°$, and with $m = 0$, for the other values of $\beta$. At $\beta = 0°$, $60°$, and $90°$, the situation is similar to the case of the $1s\sigma$ state. The agreement between the normalized exact results and the WFAT is generally good, although there is some difference in the shapes, which grows with $F$. At $\beta = 5°$ and $30°$, the exact and WFAT results

look quite different, except for the weakest field considered $F = 0.015$ at $\beta = 30°$. The difference is explained by the fact that in the leading-order approximation of the WFAT only the contribution from the dominant ionization channel can be retained. This approximation obviously fails in situations where there is no a single dominant ionization channel. This is generally the case, e.g., for $\pi^+$ states of linear molecules at small angles $\beta$. To include the contributions from both competing channels $(0,0)$ and $(0,1)$, one must simultaneously include the first-order corrections to channel $(0,0)$, which have the same order in $F$ [5]. Such an analysis of the present TMDs within the WFAT is a subject for future work [22].

Figures 16 and 17 present TMDs and their cuts for the odd $2p\pi^-$ state at several values of $\beta$ and $F$. For this state at any $\beta$, the plane $xz$ is the nodal plane of the SS eigenfunction, so the cuts are made along the ray $\varphi_k = \pi/2$. At $\beta = 0°$, the TMD for the $2p\pi^-$ state can be obtained from that for the $2p\pi^+$ state by a rotation in the $\mathbf{k}_\perp$ plane through the angle $\pi/2$, therefore the top panels in Figs. 15 and 17 actually show the same cuts. In this case the TMDs shown in Fig. 16 are $\propto \sin^2 \varphi_k$, because of the symmetry of the state. The dominant ionization channel
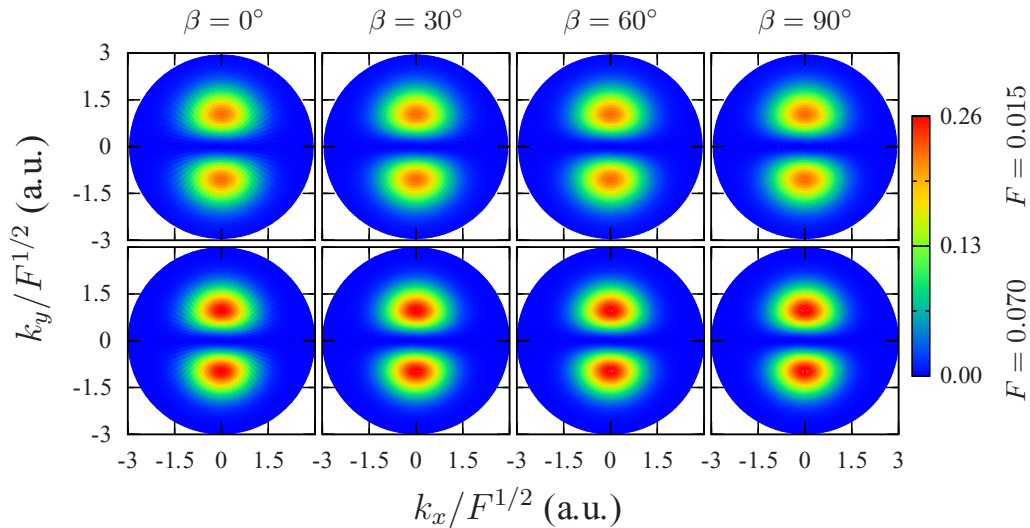
FIG. 16. (Color online) Normalized TMD $P(\mathbf{k}_\perp)/\mathcal{N}$ as a function of the scaled transverse momentum $\mathbf{k}_\perp/F^{1/2}$ for the $2p\pi^-$ state at several representative orientation angles $\beta$ and fields $F$.

for the present state is $(0,1)$, so this dependence on $\varphi_k$ should approximately hold for all values of $\beta$, according to Eq. (30). This is indeed the case. In general, the leading-order WFAT predicts the shape of the TMDs in as good agreement with the exact results as was the case for the $1s\sigma$ state. There are some deviations that, however, remain small for the values of $F$
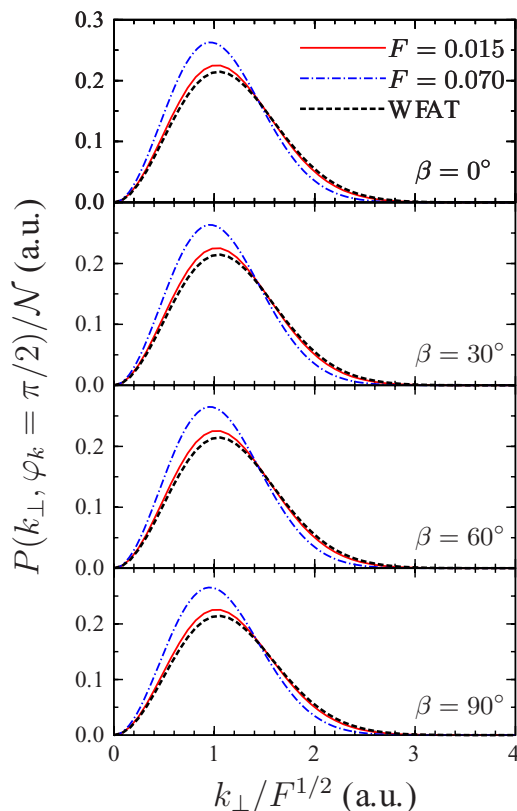


FIG. 17. (Color online) Cuts of the normalized TMDs shown in Fig. 16 along the ray $\varphi_k = \pi/2$. Dashed (black) lines: the leading-order WFAT results obtained from Eq. (30) divided by $\mathcal{N}_{as}$.

considered. Regarding the absolute magnitudes of the TMDs, the conclusion made in the end of Sec. III A 2 can be repeated here.

## IV. CONCLUSION

The implementation of the method of adiabatic expansion in parabolic coordinates, developed in Refs. [2–4] for calculating one-electron atomic and molecular SSs in a static uniform electric field, is extended to the calculation of the normalized molecular SS eigenfunction. This enables us to calculate TMDs for a general class of soft-core molecular potentials, which can be used to model arbitrarily oriented polyatomic molecules. The formulation of the method is summarized and its implementation is illustrated by calculations for the $1s\sigma$ and $2p\pi^\pm$ states of a soft-core $H_2^+$. In contrast to the atomic case [2], when the TMD is isotropic and depends only on the absolute value of the transverse momentum, in the molecular case it depends also on the direction of the momentum and generally exhibits a rich structure reflecting the symmetry of the unperturbed ionizing orbital. The results are compared with the predictions of the WFAT [4]. While for the $1s\sigma$ and $2p\pi^-$ states the shape of the TMDs is robust to the variation of field $F$ or the orientation angle $\beta$, for the $2p\pi^+$ state it undergoes a rapid transformation at small $\beta$. Such a behavior is explained within the WFAT by the existence of two competing ionization channels. Since TMD defines the photoelectron momentum distribution within the adiabatic theory [8], we believe that this finding should have implications in strong-field physics.

As was already stated in the Introduction, the SS eigenvalue and TMD amplitude are two major properties characterizing the interaction of atoms and molecules with a static electric field. Accurate numerical methods to calculate these properties, like the one developed in Refs. [2–4] and the present paper, are needed for a variety of applications. In particular, the present method provides benchmark results required to confirm the validity and gauge the accuracy of the WFAT [4,5,22] in the tunneling regime, and becomes indispensable

for calculating Stark shifts, ionization rates, and TMDs in the over-the-barrier regime. But the most interesting application of the method, the one for which it was actually developed, is in the adiabatic theory [8]. Now the theory can be implemented for molecules, and work in this direction is in progress.

[1] A. J. F. Siegert, Phys. Rev. **56**, 750 (1939).

[2] P. A. Batishchev, O. I. Tolstikhin, and T. Morishita, Phys. Rev. A **82**, 023416 (2010).

[3] L. Hamonou, T. Morishita, and O. I. Tolstikhin, Phys. Rev. A **86**, 013412 (2012).

[4] O. I. Tolstikhin, T. Morishita, and L. B. Madsen, Phys. Rev. A **84**, 053423 (2011).

[5] V. H. Trinh, O. I. Tolstikhin, L. B. Madsen, and T. Morishita, Phys. Rev. A **87**, 043426 (2013).

[6] O. I. Tolstikhin, L. B. Madsen, and T. Morishita, Phys. Rev. A **89**, 013421 (2014).

[7] F. Krausz and M. Ivanov, Rev. Mod. Phys. **81**, 163 (2009).

[8] O. I. Tolstikhin and T. Morishita, Phys. Rev. A **86**, 043417 (2012).

[9] T. Morishita, A.-T. Le, Z. Chen, and C. D. Lin, Phys. Rev. Lett. **100**, 013903 (2008).

[10] S. Minemoto, T. Umegaki, Y. Oguchi, T. Morishita, A.-T. Le, S. Watanabe, and H. Sakai, Phys. Rev. A **78**, 061402(R) (2008).

[11] C. Wang, M. Okunishi, R. R. Lucchese, T. Morishita, O. I. Tolstikhin, L. B. Madsen, K. Shimada, D. Ding, and K. Ueda, J. Phys. B **45**, 131001 (2012).

[12] H. Ohmura, N. Saito, and T. Morishita, Phys. Rev. A **89**, 013405 (2014).

[13] O. I. Tolstikhin, S. Watanabe, and M. Matsuzawa, J. Phys. B **29**, L389 (1996).

[14] K. L. Baluja, P. G. Burke, and L. A. Morgan, Comput. Phys. Commun. **27**, 299 (1982).

[15] L. D. Landau and E. M. Lifshitz, *Quantum Mechanics (Non-relativistic Theory)* (Pergamon Press, Oxford, 1977).

[16] *Handbook of Mathematical Functions*, edited by M. Abramowitz and I. A. Stegun (Dover, New York, 1972).

[17] L. B. Madsen, O. I. Tolstikhin, and T. Morishita, Phys. Rev. A **85**, 053404 (2012).

[18] L. B. Madsen, F. Jensen, O. I. Tolstikhin, and T. Morishita, Phys. Rev. A **87**, 013406 (2013).

[19] L. B. Madsen, F. Jensen, O. I. Tolstikhin, and T. Morishita, Phys. Rev. A **89**, 033412 (2014).

[20] A. M. Perelomov, V. S. Popov, and M. V. Terent'ev, Zh. Eksp. Teor. Fiz. **50**, 1393 (1966) [Sov. Phys. JETP **23**, 924 (1966)]; Zh. Eksp. Teor. Fiz. **51**, 309 (1966) [Sov. Phys. JETP **24**, 207 (1967)].

[21] The value of this energy given in Ref. [3] contains a misprint.

[22] V. H. Trinh, V. N. T. Pham, O. I. Tolstikhin, and T. Morishita (unpublished).